J Therm Spray Tech
https://doi.org/10.1007/s11666-022-01384-2

PEER REVIEWED

Suspension Flame Spray Construction of Porous Polycaprolactone/Hydroxyapatite Coatings for Marine Ecological Remediation

Zhiyuan Xu[1,2,3] · Xiaohua Feng[2,3] · Jing Huang[2,3] · Shuangjie Wu[2,3] · Ping Zhou[2,3] · Hua Li[2,3]

Submitted: 21 November 2021 / Accepted: 11 March 2022

Abstract Porous polycaprolactone (PCL)/hydroxyapatite (HA) composite coatings are deposited via suspension flame spraying for marine ecological remediation. The morphology, phase composition, chemical composition, and surface roughness are characterized by scanning electron microscopy, x-ray diffraction, Fourier transform infrared spectroscopy, and 3D optical profiler. The PCL/HA coatings exhibit porous structure, and the porosity is controlled through adjusting the content of HA. The microalgae attachment performances of *Chlorella* on the surface of 316L stainless steel substrate and the PCL/HA coatings are investigated. The PCL/HA coatings effectively increase the attachment ratio of *Chlorella*; after 7 days of incubation, the adhesion ratio is up to 69.8%. The porous structure of the PCL/HA coatings plays a significant role in promoting the attachment of microalgae, which has a valuable application in marine ecological remediation area.

Keywords marine ecological remediation · microalgae adhesion · PCL/HA composite coatings · porous structure · suspension flame spray

✉ Xiaohua Feng
xhfeng@nimte.ac.cn

[1] Henan Institute of Advanced Technology, Zhengzhou University, Zhengzhou 450003, China

[2] Zhejiang Engineering Research Center for Biomedical Materials, Cixi Institute of Biomedical Engineering, Ningbo Institute of Materials Technology and Engineering, Chinese Academy of Sciences, Ningbo 315201, China

[3] Key Laboratory of Marine Materials and Related Technologies, Zhejiang Key Laboratory of Marine Materials and Protective Technologies, Ningbo Institute of Materials Technology and Engineering, Chinese Academy of Sciences, Ningbo 315201, China

Introduction

The excessive exploitation of marine biological resources has caused a serious imbalance of marine ecosystem in the process of human economic development (Ref 1, 2). At present, the research on marine ecosystem restoration has become the concern of scientific researchers (Ref 3-7). Their findings show that microalgae has the potential to absorb nutrients in polluted sea areas, reduce water eutrophication, improve water quality, and repair water ecological chain (Ref 8-10). This bioremediation method is a practical, low-cost, and clean method (Ref 10). In addition, people can use high-fat microalgae known as "biofuel" to produce biodiesel (Ref 7).

Coral reefs are the habitat of microalgae (Ref 11, 12). However, since 1957, about half of the area of global coral reefs has been decreased, and about 60% of the biodiversity bred by coral reefs has dropped (Ref 1, 4, 5). Therefore, research on artificial coral reefs for marine ecological restoration is arising. Microalgae attachment to the surface of solid substrate (such as coral reef) is an important immobilization technology (Ref 13-15). Through this technology, building a substrate or coating to be suitable for microalgae growth is one of the effective solutions to the above problems (Ref 16-19). For example, porous artificial ceramic reefs prepared by sintering method (Ref 17), or bionic coral reefs fabricated by 3D printing technology (Ref 13) can provide a good growth matrix for microalgae. The surface properties of styrene acrylic film on stainless steel substrate by tape casting method (Ref 16) or polytetrafluoroethylene (PTFE) film deposited on the glass by spraying and sintering methods (Ref 20) may also affect the growth of microalgae. Some researchers also directly design surface structure of substrate to investigate the effects of surface wettability and roughness on the

Published online: 12 April 2022

growth of microalgae (Ref 21-24). These research works have generally demonstrated that the roughness of substrate or coating surface is the main factor affecting the attachment of microalgae, since rough surface can provide more attachment points for microalgae than the smooth one.

In addition to the choice of immobilization technology, the choice of coating materials must also be considered. Hydroxyapatite (HA), a type of CaP-based bio-ceramics, has good biocompatibility (Ref 25-27). However, presently there are few reports about the growth promotion of microalgae upon HA coating materials. The preparation methods of HA coating or film include hydrothermal method (Ref 28), cold spraying method (Ref 29), plasma spraying method (Ref 30), suspension flame spraying method (Ref 31), etc. The selection of methods is usually determined by the properties of original materials (Ref 32). In this paper, HA coating is deposited on stainless steel substrate by suspension flame spraying from HA powder synthesized by liquid-phase precipitation method (Ref 33), and then the effects of its surface structure and composition on the growth of microalgae are investigated. Because of the difference of expansion coefficient between HA material and stainless steel substrate (Ref 31), HA coating may have poor adhesion to stainless steel substrate. In order to overcome the deficiency of mechanical properties, polycaprolactone (PCL) with good biocompatibility (Ref 34) is proposed to be used as the binder to improve the mechanical properties between coating and substrate.

Materials and Methods

Material Preparation

HA powders were synthesized by solution precipitation method: 2.5 mol/L $Ca(NO_3)_2$ (AR, Sinopharm Chemical Reagent Co., Ltd., China) and 1.5 mol/L $(NH_4)_2HPO_4$ (97%, Sinopharm Chemical Reagent Co., Ltd., China) were prepared as raw materials. NH_4OH (AR, Shanghai Aladdin Biochemical Technology Co., Ltd., China) was used to adjust the pH value of the two raw materials for reaction solutions. The reaction equation can be expressed as (Ref 33)

$$6(NH_4)_2HPO_4 + 10Ca(NO_3)_2 + 8NH_4OH \rightarrow Ca_{10}(PO_4)_6(OH)_2 + 20NH_4NO_3 + 6H_2O$$

After reaction, a slurry was freeze-dried to obtain white HA powders. PCL was purchased from Shanghai Macklin Biochemical Co., Ltd., China. F/2 medium (Shanghai Guangyu Biological Technology Co., Ltd., China) was prepared by nitrate ($NaNO_3$, 75 g/m3), phosphate ($NaH_2PO_4 \cdot H_2O$, 5 g/m^3), trace metal ($FeCl_3 \cdot 6H_2O$, 3.15 g/m^3; $Na_2EDTA \cdot 2H_2O$, 4.36 g/m^3; $MnCl_2 \cdot 4H_2O$, 180 mg/m^3), and vitamin (thiamine HCl, 200 mg/m^3; cyanocobalamin, 10 mg/m^3; biotin, 100 g/m^3) (Ref 35).

Coating Preparation

Ten grams of PCL powder was added to 100 mL anhydrous ethanol to form PCL suspension, 5 g HA powder was added to 100 ml anhydrous ethanol to form HA suspension, and different proportions of HA and PCL powders (the two powders are 10g in total) were dispersed in 100 ml anhydrous ethanol to fabricate PCL/HA mixture suspensions. The prepared PCL coating, PCL/10wt%HA coating, PCL/20wt%HA coating, and PCL/30wt%HA coating are marked as P0, P1, P2, and P3, respectively. The suspensions were sprayed on the sand-blasted 316L SS surface after being stirred with a magnetic stirrer at 400 rpm for 2 hours. CastoDyn DS 8000 system is employed for suspension flame spraying with C_2H_2 pressure 0.1 MPa, O_2 pressure 0.5 MPa, feed rate 25 ml/min, and spraying distance 15 cm.

Sample Characterization

The morphologies of PCL, HA nanoparticles, and coatings were observed by scanning electron microscope (SEM, Regulus8230, Hitachi, Japan) and transmission electron microscope (TEM, JEM-2100, JEOL Ltd., Japan). X-ray diffraction (XRD, D8 ADVANCE, Bruker, Germany) was used to determine the crystal structure of powders and coatings with Cu Kα radiation at 40 kV and scan rate of 0.047 °/s over the range of 20-60°. The chemical composition of coatings was analyzed by Fourier transform infrared spectroscopy (FTIR, Nicolet iS50, Thermo Fisher Scientific, USA). Three-dimensional images of surface roughness (Ra, μm) were characterized by 3D optical profilometer (3DOP, UP-Lambda, Rtec Instruments, USA).

Characterization of Microalgae Adhesion on the Coatings

Chlorella was employed to characterize the adhesion behavior of microalgae on the different coatings. Firstly, *Chlorella* solution was added into F/2 medium and subsequently cultivated in an incubator at 25°C. The concentration of *Chlorella* solution was estimated by spectrophotometer (SpectraMax 190, Molecular Devices, USA) at a wavelength of 450 nm and marked as optical density (OD_{450nm}). In the next step, four parallel samples were set for each coating. The samples were dipped into the *Chlorella* solution (OD_{450nm} = 0.8) for 1, 3, 5, and 7 days. At specific time, the *Chlorella* solution was removed and the samples were washed with deionized water to

remove the unattached *Chlorella* and then immersed in 2.5% glutaraldehyde at 4°C for 2 hours to fix the attached *Chlorella*. Finally, the fluorescence images of microalgae were obtained by confocal laser scanning microscopy (CLSM, TCS SP8, Leica, Germany). The adhesion ratios were calculated by using software ImageJ (version 1.53a).

Statistical Analysis

All statistical analyses were conducted with software IBM SPSS Statistics (version 26) at a confidence level of 95%. One-way analysis of variance (ANOVA) test was conducted to assess the difference between different groups.

Results and Discussion

SEM image (Fig. 1a) shows that the majority of HA powder is consisted of agglomerated microparticles (highlighted by white circle) with the size of 0.3 ~ 3 μm and part of them is flaky (highlighted by black rimmed). TEM image of HA powder exhibits that it is of rodlike shaped with 15 ~ 25 nm in diameter and 50 ~ 100 nm in length. The agglomerated powders are formed by the aggregation of these nano-rodlike-shaped HA particles. The PCL powders are irregular block particles with a size of 20 ~ 70 μm (Fig. 1b).

Crystal structure of HA powders, pure HA coating, and the PCL/HA composite coatings on 316L SS substrate are analyzed according to the XRD patterns (Fig. 2). The HA powder prepared through solution precipitation method conforms to the characteristic peaks marked by HA powder diffraction card PDF 09-0432, which means that HA nanopowder with high purity can be obtained by this method. In PCL/HA composite coatings, all characteristic peaks of HA appear, indicating that HA has no phase transition and retains the same phase of the original powders in the process of suspension flame spraying. With the increase in HA content in the PCL/HA composite coatings, the intensity of HA diffraction peaks slightly increases (Fig. 2d-f); the peak of 43.5° represents the characteristic peak of 316L substrate, which has a certain influence on the characteristic peak strength of HA in the coatings. All the coatings contain this characteristic peak of the substrate, which means the density or thickness of the coating is not enough; x-ray may penetrate the coating and measure the peaks of substrate. In addition, no new phase is found in the composite coatings, indicating that HA does not decompose into other chemical such as tri–calcium phosphate or octa–calcium phosphate during thermal spraying. XRD diffraction peaks for PCL are not observed due to its amorphous state (Ref 36).

The FTIR spectrums of P0, P1, P2, and P3 coatings show the peaks at 2959, 2849, and 1726 cm^{-1} position (Fig. 3), which means the asymmetric CH_2 stretching, symmetric CH_2 stretching, and carbonyl absorption peaks, respectively, indicating that the PCL retains original

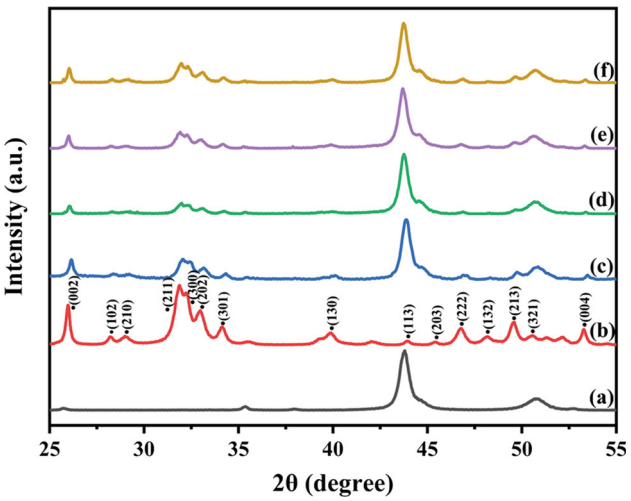

Fig. 2 XRD patterns of (a) 316L substrate, (b) HA powders, (c) HA coating, (d) P1, (e) P2, and (f) P3 coatings

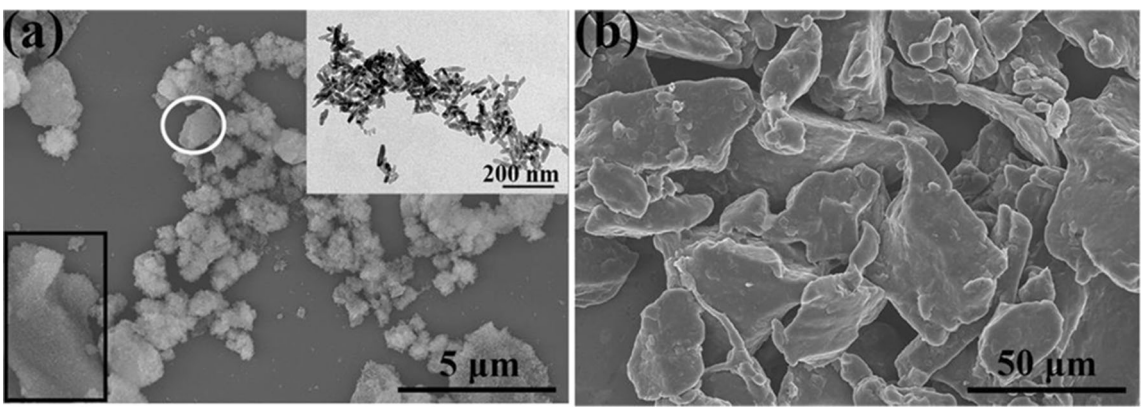

Fig. 1 SEM and TEM images (a) of HA powders, and SEM image (b) of PCL powders

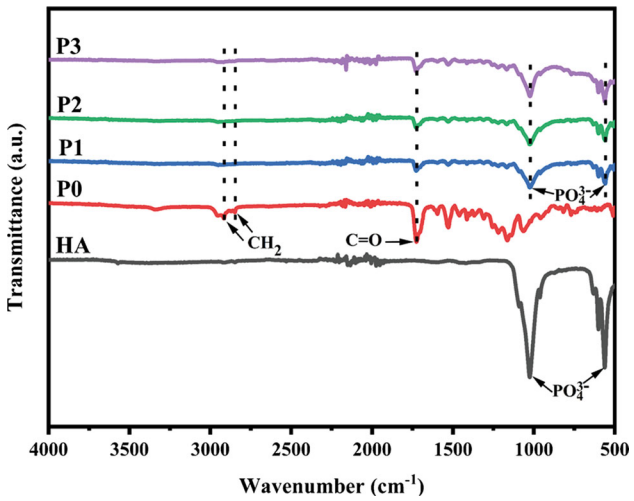

Fig. 3 FTIR spectra of HA, P0, P1, P2, and P3 coatings

components in the composite coating during the thermal spraying process. The FTIR spectrums of the HA, P1, P2, and P3 coatings show the peaks at 560 cm^{-1} and 1044 cm^{-1}, which represents the PO_4^{3-} vibration absorption peak (Ref 37), indicating that the HA is remained in the composite coating; this analysis result is consistent with the XRD conclusion.

Surface morphology and cross section view of HA, P0, P1, P2, and P3 are shown in Fig. 4. The surface of pure PCL coatings is relatively smooth and has no obviously visible pores (Fig. 4b-1-2). At high magnification image of pure HA coating, it is obvious that the coating contains unmelted HA particles (Fig. 4a-2) (Ref 38). On the contrary, P1, P2, and P3 coatings show obvious porous structure (Fig. 4c-e-1, highlighted by white arrow). The surface porosities of these composite coatings are calculated by software Image J; the porosity ratio is about 7.6% for P1, 20.1% for P2 and 22.2% for P3 coatings, respectively. The surface porosity of the PCL/HA composite coatings is increasing with the increasing HA content. During the thermal spraying process, the deposition states of HA and PCL are different due to the different melting points (HA 1500°C; PCL 59-64°C) and different densities (HA 3.16g/cm^3; PCL 1.02g/cm^3) (Ref 39, 40). Generally, the unmelted or semi-molten HA particles will be embedded inside the melting PC coating and formed a protrusion or hole surface, which may result in roughness surface or porous surface. Moreover, the HA wrapped in PCL droplets may restrict flow of liquid PCL into pores, and the roughness and pore become obviously with the increasing of HA content (Fig. 4c-e-2) (Ref 41). Therefore, the porosities of the PCL/HA composite coatings are increasing with the increase in the HA content in suspension. The thickness of HA coating can be measured from the cross-sectional morphology, P0, P1, P2, and P3 coatings is about 4-9, 22-33, 19-25, 27-33, and 41-43μm, respectively (Fig. 4a-e-3). The amount of HA particles wrapped in PCL increases with the increase in the amount of powder in original powder, so the thickness of the coating gradually increases. However, as the amount of HA powder in coating increases, the adhesion between the coating and the substrate deteriorates and the coating is easy to flake off. At present, HA original powder content is only added to 30%, to ensure that adhesion of the coating and matrix binding force is more than 10MPa.

The adhesion properties of *Chlorella* attached on the surface of 316L and all coatings after 1, 3, 5, and 7 days are investigated through CLSM technology. For all the coatings, the adhesion amount of the *Chlorella* is increasing with the increase in adhesion time, and the distribution of the *Chlorella* on the coatings surface is uniform (Fig. 5). However, the adhesion amount on the composite coating is significantly higher than the *Chlorella* on 316L substrate, when HA and P0 coatings have the same adhesion days. Furthermore, with the increase in HA content, the adhesion increment of *Chlorella* on composite coating is also increasing. P2 and P3 coatings show a good ability to promote the growth microalgae.

The adhesion rate of microalgae over time is calculated by software Image J. The adhesion ratios of *Chlorella* on the 316L substrate, HA, and P0 coating keep a low value after 7 days of incubation, about 6.17, 7.2, and 16.1%, respectively. However, for P1, P2, and P3 coatings, the adhesion ratio reaches 46.1, 51.4, and 69.8%, respectively (Fig. 6a). The order of *Chlorella* adhesion ratios on these coatings is P3 > P2 > P1 > P0 > HA > 316L. Through the statistical analysis of many samples, the adhesion amount of *Chlorella* significantly increases on the surface of P1, P2, and P3 (Fig. 6b). These results indicate that the PCL/HA coatings prepared by suspension flame spraying promote prominently the adhesion of *Chlorella.*

In order to analyze the adhesion behavior of *Chlorella* on the composite coating, we observe the surface of P2 coating after 7 days *Chlorella* incubated. It can be clearly found that *Chlorella* are not attached to the smooth areas (highlighted by the black oval) (Fig. 7a), but in the protruding position of the coating (highlighted by the white arrow) (Fig. 7b), the protruding parts increase the surface roughness and consequently enhance microorganism adhesion as the anchoring points for *Chlorella* (Ref 42-44). Moreover, some *Chlorella* are observed on pores of the surface (highlighted by the black arrow) (Fig. 7b). The micropores may encapsulate microalgae when they are

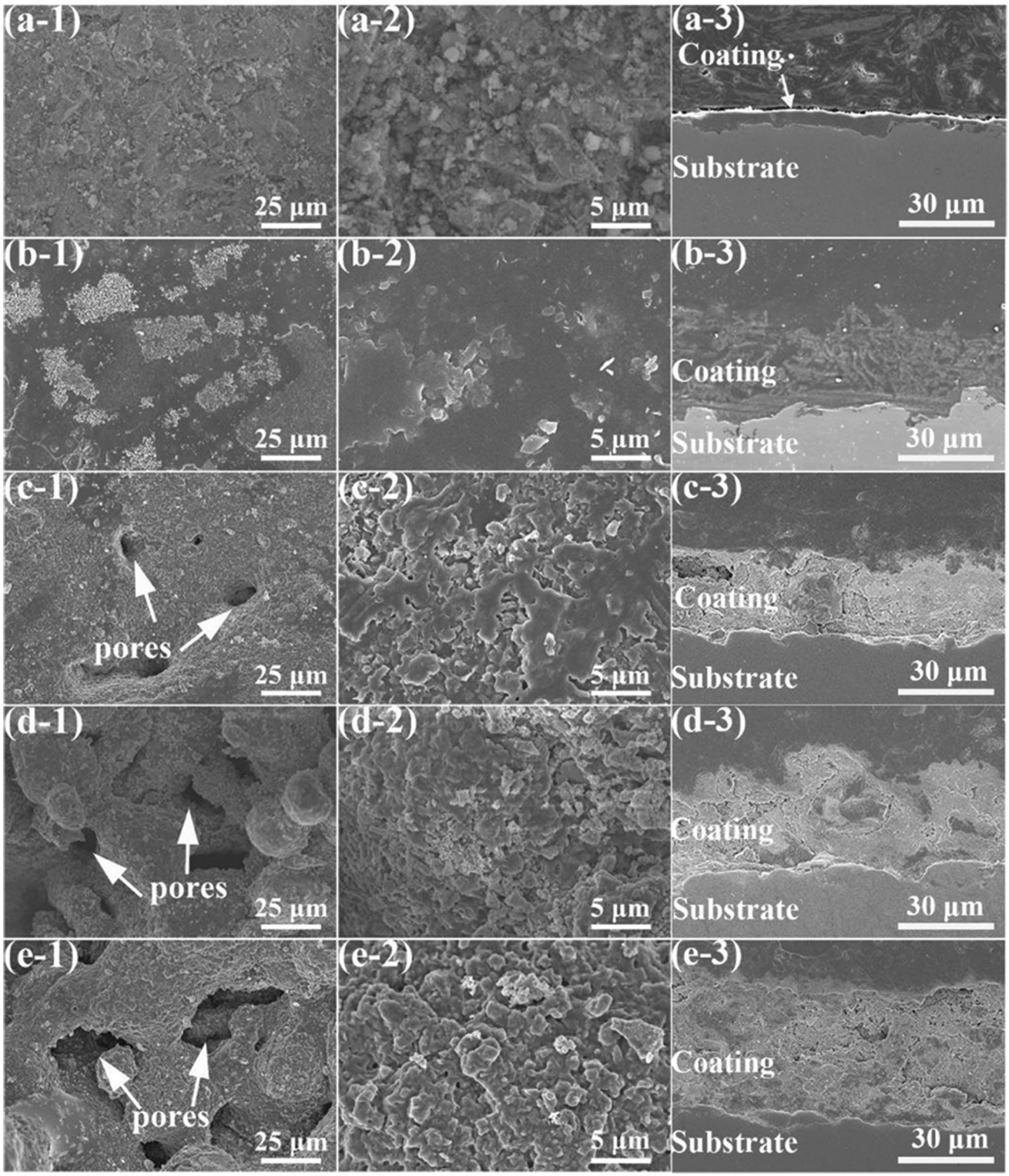

Fig. 4 SEM image of surface morphologies (1: low magnification, 2: high magnification) and (3) cross section image of (a) HA, (b) P0, (c) P1, (d) P2, and (e) P3 coatings.

attached to the surface; this surface feature influences the attachment and colonization of the microorganism (Ref 20, 45-48). Special surface structures such as microgroove (Ref 24), mesh pore (Ref 22), ridge, pillar, and groove (Ref 49) often provide larger attachment points for microalgae, which is conducive to the attachment of the microalgae. In

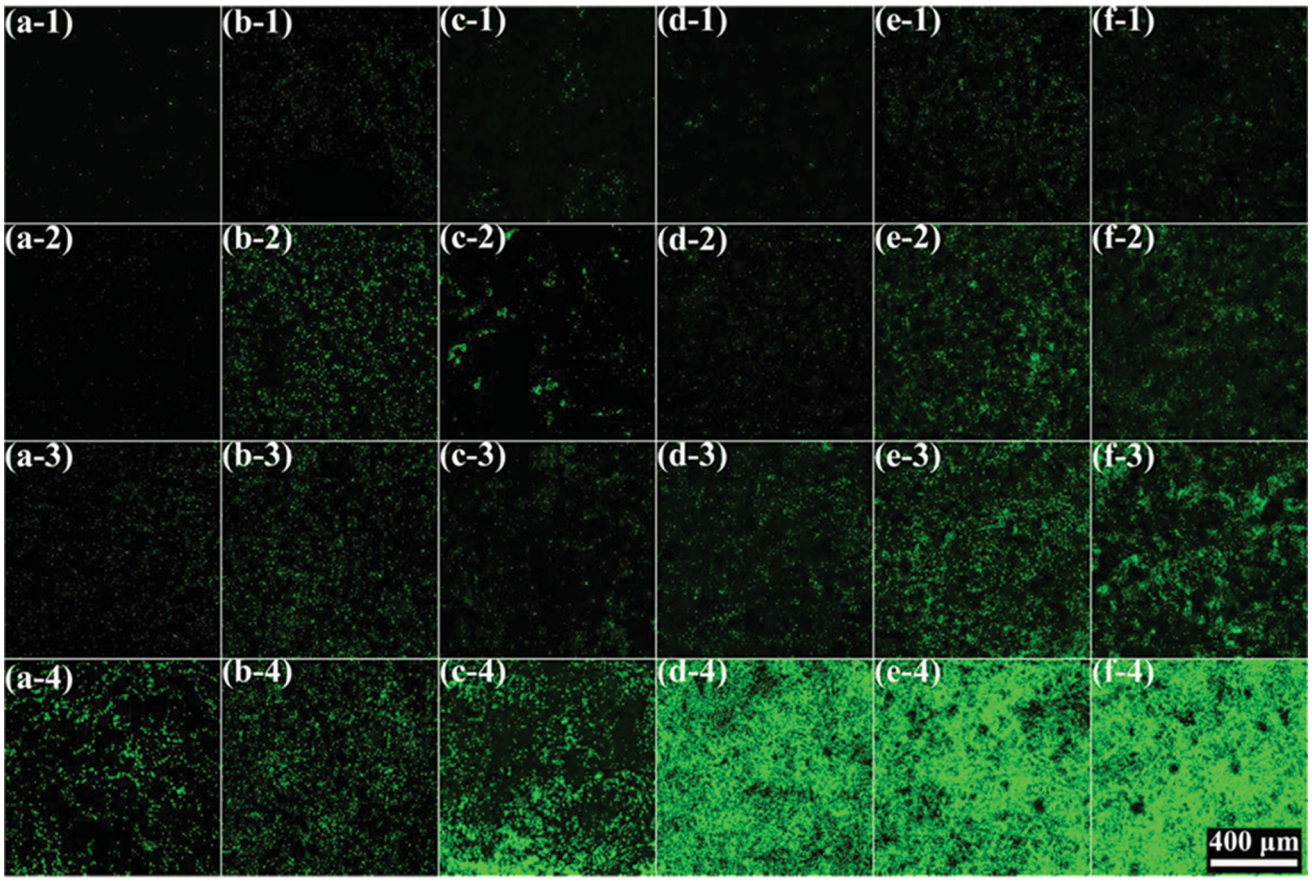

Fig. 5 CLSM images of *Chlorella* adhesion on (a) 316L, (b) HA, (c) P0, (d) P1, (e) P2, and (f) P3 coatings (1 means 1 day incubated, 2 means 3 days, 3 means 5 days, and 4 means 7 days, scale bar 400 μm)

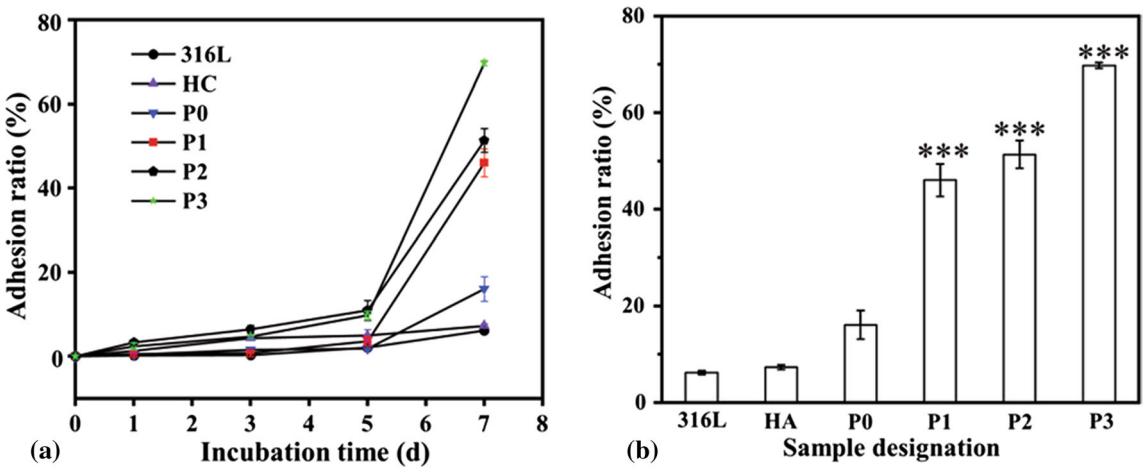

Fig. 6 (a) Variation chart of adhesion rate with time, (b) statistical chart of adhesion rate after 7 days *Chlorella* incubated, $***p < 0.05$ compared with P0. Error bars are shown as ± SD ($n = 4$)

short, porous structure of the composite coatings enhances microalgae attachment and is the crucial factor for colonization of microalgae.

The three-dimensional images further indicate the surface rough structures of all coatings (Fig. 8). The surface of P0 coating is very smooth, which is consistent with SEM image (Fig. 4b). During the spraying process, PCL is melted into liquid under a high temperature (up to 2000°C) of flame (Ref 50) and then impacted to the substrate to form a flat surface. Therefore, the roughness of the P0

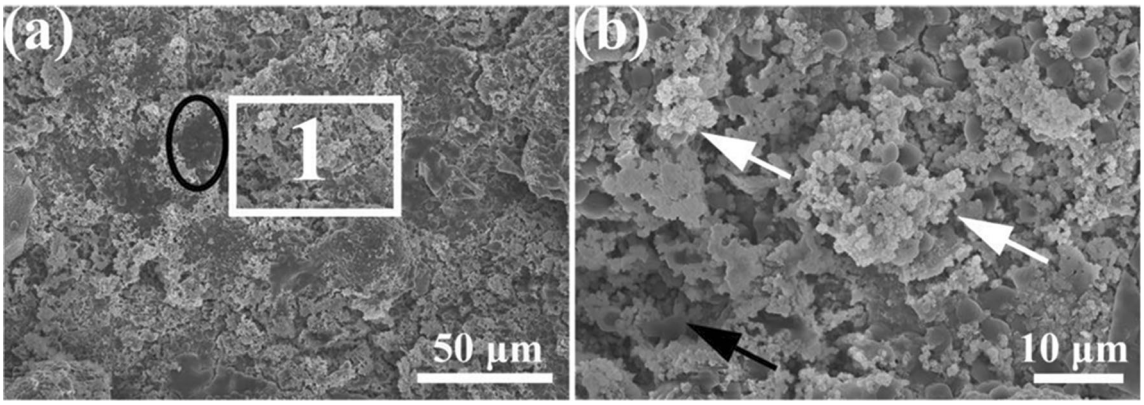

Fig. 7 SEM images of *Chlorella* adhered on P2 coating after 7 days of incubation, (b) enlarged view of the selected area 1 in (a)

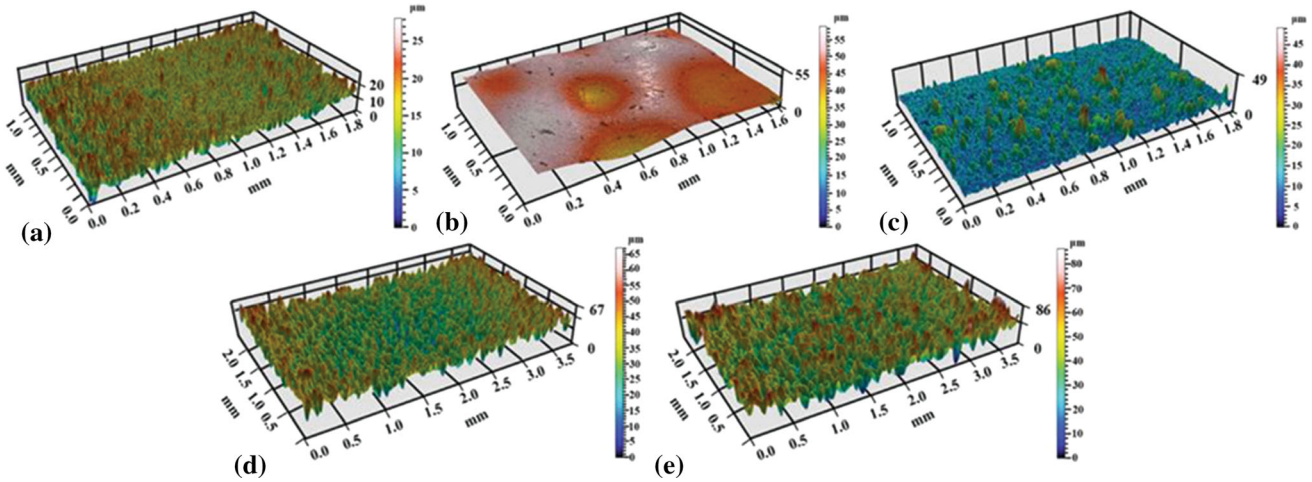

Fig. 8 Three-dimensional images of roughness for (a) HA, (b) P0, (c) P1, (d) P2, and (e) P3 coatings

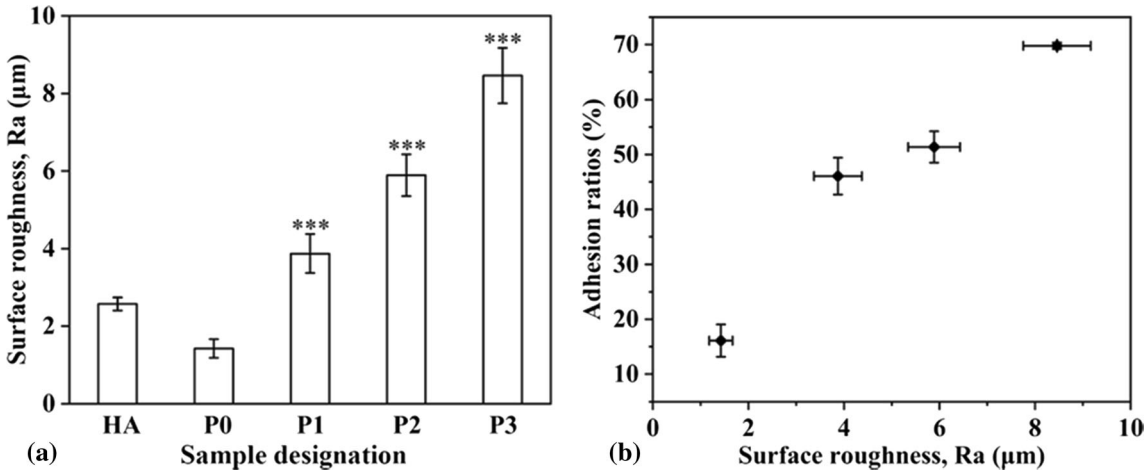

Fig. 9 (a) Surface roughness (Ra, μm) of all coatings, error bars are shown as ± SD (n = 3), ***p<0.05 compared with the P0 coating; (b) variation curve between adhesion rate and surface roughness of P0, P1, P2, and P3, error bars of the adhesion ratios and surface roughness are shown as ± SD (n = 4 and n=3, respectively)

coating is about 1.42 ± 0.24 μm (Fig. 9b). Due to the high melting point of HA, during thermal spraying, HA particles are half-melted; therefore, the HA particles on the substrate present a rough surface. The surface roughness of HA coating is about 2.57 ± 0.17 μm (Fig. 9a). May be due to the alternating deposition of liquid and solid particles, the

composite coatings show more pores (Fig. 4c-e).The roughness of P1, P2, and P3 composite coatings is about 3.87 ± 0.50 μm, 5.89 ± 0.54 μm, and 8.46 ± 0.71 μm, respectively. Compared with P0 coating, the roughness of composite coating increases with the increase in HA contents.

The linear fitting of the adhesion ratios of P0, P1, P2, and P3 coatings after the 7th incubation day with the surface roughness is plotted in Fig. 9(b). A linear increment of adhesion ratios is obtained with the increase in the surface roughness, which means that the surface roughness has an important effect on the adhesion behavior of micro-algae; the results are consistent with other reports.

Conclusion

PCL/HA composite coatings are fabricated through suspension flame spraying, and the coatings have typical porous structure with a rough surface. The contents of HA of the coatings will adjust the surface roughness and porosity. The porous structure can enhance the attachment and colonization of *Chlorella*. There is a linear growth relationship between coating surface roughness and microalgae adhesion rate. In the composite coatings, the roughness of P3 coating can reach 8.46 and the *Chlorella* adhesion ratio on this coating is about 69.8% after incubation for 7 days. The study results suggest that PCL/HA composite coatings prepared by suspension flame spraying may have prospect in the field of marine ecological remediation.

Acknowledgment This work was supported by the Chinese Academy of Sciences Key Project (ZDRW-CN-2019-3), the S&T Innovation 2025 Major Special Programme of Ningbo (2018B10054), and K.C. Wong Education Foundation (Grant # GJTD-2019-13).

References

1. M.O. Lee, S. Otake and J.K. Kim, Transition of artificial reefs (ARs) research and its prospects, *Ocean Coast. Manag.*, 2018, **154**, p 55-65.
2. T. Chopin et al., Developing Porphyra/salmon integrated aquaculture for bioremediation and diversification of the aquaculture industry, *J. Appl. Phycol.*, 1999, **11**, p 463-472.
3. R.L. Morris et al., From grey to green: Efficacy of eco-engineering solutions for nature-based coastal defence, *Glob. Chang. Biol.*, 2018, **24**(5), p 1827-1842.
4. X. Yang et al., Effects of artificial reefs on the meiofaunal community and benthic environment - A case study in Bohai Sea China, *Mar. Pollut. Bull.*, 2019, **140**, p 179-187.
5. V. Komyakova et al., Assessing the performance of artificial reefs as substitute habitat for temperate reef fishes: Implications for reef design and placement, *Sci. Total. Environ.*, 2019, **668**, p 139-152.
6. C.A. Layman and J.E. Allgeier, An ecosystem ecology perspective on artificial reef production, *J. Appl. Ecol.*, 2020, **57**(11), p 2139-2148.
7. L.T. Nguyen, P.D. Tran and K.Q. Nguyen, An effectiveness of artificial coral reefs in the restoration of marine living resources, *Reg. Stud. Mar. Sci.*, 2022, **49**, p 102143.
8. K. Verma, P.K. Kumar, S.V. Krishna and V. Himabindu, Phycoremediation of sewage-contaminated lake water using microalgae-bacteria co-culture, *Water, Air, Soil Pollut.*, 2020, **231**(6), p 1-16.
9. Q. Emparan, R. Harun and M.K. Danquah, Role of Phycoremediation for nutrient removal from wastewaters: A review, *Appl. Ecol. Environ. Res.*, 2019, **17**(1), p 889-915.
10. Z. Yu et al., Bioremediation and fodder potentials of two *Sargassum* spp. in coastal waters of Shenzhen South China, *Mar Pollut. Bull.*, 2014, **85**(2), p 797-802.
11. L.B. Zhang et al., An artificial oyster-shell reef for the culture and stock enhancement of sea cucumber, *Apostichopus japonicus*, in shallow seawater, *Aquac. Res.*, 2015, **46**(9), p 2260-2269.
12. S.M. Jung et al., A new approach to the restoration of seaweed beds using *Sargassum fulvellum*, *J. Appl. Phycol.*, 2020, **32**(4), p 2575-2581.
13. D. Wangpraseurt et al., Bionic 3D printed corals, *Nat Commun*, 2020, **11**(1), p 1748.
14. Z.J. Dong et al., Artificial reefs for sea cucumber aquaculture confirmed as settlement substrates of the moon jellyfish Aurelia coerulea, *Hydrobiologia*, 2018, **818**(1), p 223-234.
15. E. Higgins et al., Benthic community succession on artificial and natural coral reefs in the northern Gulf of Aqaba Red Sea, *PLoS ONE*, 2019, **14**(2), p e0212842.
16. J. Tang et al., Impacts of surface wettability and roughness of styrene-acrylic resin films on adhesion behavior of microalgae Chlorella sp, *Colloids Surf. B: Biointerf.*, 2021, **199**, p 111522.
17. M. A. Kalam, T. Mieno, and B.E. Casareto, Development of artificial reefs using environmentally safe ceramic material. J. Ecosyst. Ecography. **08**(01) (2018)
18. J. X. Wen, et al., Fabrication of Porous Aluminum Coating by Cored Wire Arc Spray for Anchoring Antifouling Hydrogel Layer. J. Thermal Spray Technol. (2021)
19. J. Mallela, B.C. Milne and D. Martinez-Escobar, A comparison of epibenthic reef communities settling on commonly used experimental substrates: PVC versus ceramic tiles, *J. Exp. Mar. Biol. Ecol.*, 2017, **486**, p 290-295.
20. Y.P. Zheng et al., Effects of wettability on the growth of Scenedesmus obliquus biofilm attached on glass surface coated with polytetrafluoroethylene emulsion, *Int. J. Hydrogen Energy*, 2016, **41**(46), p 21728-21735.
21. R. Sekar et al., Laboratory Studies on Adhesion of Microalgae to Hard Substrates, *Hydrobiologia*, 2004, **512**, p 109-116.
22. M. Gross et al., Effects of the surface physico-chemical properties and the surface textures on the initial colonization and the attached growth in algal biofilm, *Biotechnol. Biofuels*, 2016, **9**, p 38.
23. J. Cao et al., A preliminary study of the effect of surface texture on algae cell attachment for a mechanical-biological energy manufacturing system, *J. Manuf. Sci. Eng*, 2009, **131**, p 1-4.
24. Y. Huang et al., Enhancing microalgae biofilm formation and growth by fabricating microgrooves onto the substrate surface, *Bioresour. Technol.*, 2018, **261**, p 36-43.
25. B. Dikici et al., Synthesis of biphasic calcium phosphate (BCP) coatings on β-type titanium alloys reinforced with rutile-TiO_2 compounds: adhesion resistance and in-vitro corrosion, *J. Sol-Gel. Sci. Technol.*, 2018, **87**(3), p 713-724.
26. M. Topuz, B. Dikici and M. Gavgali, Titanium-based composite scaffolds reinforced with hydroxyapatite-zirconia: Production,

mechanical and in-vitro characterization, *J. Mech. Behav. Biomed. Mater.*, 2021, **118**, p 104480.
27. A.M. Deliormanli and R. Konyali, Bioactive glass/hydroxyapatite- containing electrospun poly (ε-Caprolactone) composite nanofibers for bone tissue engineering, *J. Aust. Ceram. Soc.*, 2018, **55**(1), p 247-256.
28. O. Yigit et al., One-step synthesis of nano-hydroxyapatite/graphene nanosheet hybrid coatings on ti6al4v alloys by hydrothermal method and their in-vitro corrosion responses, *Surf. Coat. Technol*, 2020, **394**, p 1-10.
29. Y. Liu et al., Hydroxyapatite/graphene-nanosheet composite coatings deposited by vacuum cold spraying for biomedical applications: inherited nanostructures and enhanced properties, *Carbon*, 2014, **67**, p 250-259.
30. Y.W. Gu et al., Activity of plasma sprayed yttria stabilized zirconia reinforced hydroxyapatite/Ti-6Al-4V composite coatings in simulated body fluid, *Biomaterials*, 2004, **25**(16), p 3177-3185.
31. C.L. Yang et al., Development of novel thermal sprayed hydroxyapatite-rare earth (HA-Re) coatings for potential antimicrobial applications in orthopedics, *J. Therm. Spray Technol.*, 2021, **30**(4), p 886-897.
32. B. Dikici and M. Topuz, Production of annealed cold-sprayed 316L stainless steel coatings for biomedical applications and their in-vitro corrosion response, *Protect. Metals Phys. Chem. Surf.*, 2018, **54**(2), p 333-339.
33. I. Mobasherpour et al., Synthesis of nanocrystalline hydroxyapatite by using precipitation method, *J. Alloy. Compd.*, 2007, **430**(1-2), p 330-333.
34. J.M. Vion et al., Synthesis, characterization, and miscibility of caprolactone random copolymers, *Macromolecules*, 1986, **19**, p 1828-1838.
35. R.R.L Guillard, Culture of Phytoplankton for Feeding Marine Invertebrates. Cult. Mar. Invertebr. Anim, 29-60 (1975)
36. S.C. Jiang et al., Crystallization behavior of PCL in hybrid confined environment, *Polymer*, 2001, **42**, p 3901-3907.
37. X.D. Wu et al., Preparation of Mesoporous Nano-Hydroxyapatite Using a Surfactant Template Method for Protein Delivery, *J. Bionic. Eng.*, 2012, **9**(2), p 224-233.
38. H.L. Yao et al., Microstructures, mechanical properties and electrochemical behaviors of nano-structured HA/Ti composite coatings deposited by high-velocity suspension flame spray (HVSFS), *Ceram. Int.*, 2018, **44**(11), p 13024-13030.
39. N. Sanpo et al., Antibacterial property of cold-sprayed HA-Ag/PEEK coating, *J. Therm. Spray Technol.*, 2008, **18**(1), p 10-15.
40. J.M. Chen et al., Solution extrusion additive manufacturing of biodegradable polycaprolactone, *Appl. Sci.*, 2020, **10**(9), p 3189.
41. M.J. Kim and Y.H. Koh, Synthesis of aligned porous poly(epsilon-caprolactone) (PCL)/hydroxyapatite (HA) composite microspheres, *Mater. Sci. Eng. C Mater. Biol. Appl.*, 2013, **33**(4), p 2266-2272.
42. K. Balani et al., Tribological behavior of plasma-sprayed carbon nanotube-reinforced hydroxyapatite coating in physiological solution, *Acta. Biomater.*, 2007, **3**(6), p 944-951.
43. J.A. Gan and C.C. Berndt, Nanocomposite coatings: thermal spray processing, microstructure and performance, *Int. Mater. Rev.*, 2014, **60**(4), p 195-244.
44. M.F. Hassan, H.P. Lee and S.P. Lim, Effects of shear and surface roughness on reducing the attachment of *Oscillatoria* sp. filaments on substrates, *Water Environ. Res.*, 2012, **84**(9), p 744-752.
45. L. Xiao et al., Topographic cues guide the attachment of diatom cells and algal zoospores, *Biofouling*, 2018, **34**(1), p 86-97.
46. S.N. Genin, J.S. Aitchison and D.G. Allen, Design of algal film photobioreactors: material surface energy effects on algal film productivity, colonization and lipid content, *Bioresour. Technol.*, 2014, **155**, p 136-143.
47. M. Melo et al., Chlorella vulgaris (SAG 211-12) biofilm formation capacity and proposal of a rotating flat plate photobioreactor for more sustainable biomass production, *J. Appl. Phycol.*, 2017, **30**(2), p 887-899.
48. J.W. Arnold and G.W. Bailey, Surface finishes on stainless steel reduce bacterial attachment and early biofilm formation: scanning electron and atomic force microscopy study, *Poult. Sci.*, 2020, **79**, p 1839-1845.
49. Y. Cui, W.Q. Yuan and J. Cao, Effects of surface texturing on microalgal cell attachment to solid carriers, *Int. J. Agric. & Biol. Eng.*, 2013, **6**(4), p 44-54.
50. J. Tikkanen et al., Characteristics of the liquid flame spray process, *Surf. Coat. Technol.*, 1997, **90**, p 210-216.